Interpretable Machine Learning for Ambient Temperature Prediction: Insights from SHAP, ICE, PDP, and ALE

Hirushan Sajindra[1,2], Thilina Abekoon[2], Salani Buthpitiya[3], Yasitha Alahakoon[4], Namal Rathnayake[5], Komali Kantamaneni[6,7], and Upaka Rathnayake[1,*]

[1]Faculty of Engineering and Design, Atlantic Technological University, Sligo, F91 YW50, Ireland
[2]Water Resources Management and Soft Computing Research Laboratory, Millennium City, Athurugiriya, 10150, Sri Lanka
[3]Department of Chemistry, Faculty of Science, University of Kelaniya, 11600, Sri Lanka
[4]Department of Civil Engineering, Faculty of Engineering, University of Peradeniya, Peradeniya, Sri Lanka
[5]Advanced Institute for Marine Ecosystem Change (WPI-AIMEC), Japan Agency for Marine-Earth Science and Technology (JAMSTEC), Yokohama 236-0001, Japan
[6]United Nations-SPIDER-UK Regional Support Office, Preston PR1 2HE, United Kingdom
[7]School of Engineering and Computing, University of Lancashire, Preston PR1 2HE, United Kingdom
Email: hirushansajindra96@gmail.com (H.S.); thilinaabekoon@gmail.com (T.A.); skbuthpitiya@gmail.com (S.B.); yasithaalahakoon98@gmail.com (Y.A.); namalr@jamstec.go.jp (N.R.); KKantamaneni@uclan.ac.uk (K.K.); upaka.rathnayake@atu.ie (U.R.)
*Corresponding Author
Manuscript received August 29, 2025; revised December 15, 2025; accepted March 19, 2026; published May 16, 2026

***Abstract*—Accurate ambient temperature prediction is essential for climate monitoring, urban planning, and environmental management, particularly in regions experiencing rapid climatic variability such as Sri Lanka. This study investigates the application of explainable machine learning models for short-term ambient temperature prediction in Battaramulla, Sri Lanka. Five regression algorithms-K-Nearest Neighbors (KNN), Decision Tree (DT), Random Forest (RF), Support Vector Regression (SVR), and Histogram-based Gradient Boosting Regressor (HGBR) were evaluated using 14 meteorological and environmental predictors, including temporal variables, relative humidity, solar radiation, rainfall, wind speed, and air pollutant concentrations (CO_2, NO_x, CH_4, O_3, CO, $PM_{2.5}$, and PM_{10}). Among the models tested, HGBR demonstrated superior predictive performance, achieving R^2 values of 1.00 (training) and 0.96 (testing), with corresponding mean squared error values of 0.01 and 0.11. Model interpretability was examined using SHapley Additive exPlanations (SHAP), Partial Dependence Plots (PDP), Individual Conditional Expectation (ICE) analyses, and Accumulated Local Effects (ALE), which identified several features as the most influential predictors. Model validation using 192 real-time observations showed close agreement between predicted and measured temperatures, although the evaluation was limited to a single location and time period. A web-based application, 'Therma', was developed to facilitate practical deployment of the model for localized temperature estimation. Overall, this study demonstrates the utility of explainable machine learning for localized climate prediction while highlighting the need for broader spatiotemporal validation in future work.**

***Keywords*—ambient temperature, explainable artificial intelligence, Histogram-Based Gradient Boosting Regression (HGBR), prediction**

I. Introduction

Global warming refers to the gradual increase in the average surface temperature of the Earth, primarily driven by human activities such as fossil fuel combustion, deforestation, and industrial processes [1, 2]. This increase in temperature is a key driver of climate change, leading to severe consequences, including sea-level rise, more frequent and intense weather events, and widespread ecosystem disruptions. McCulloch *et al.* [3] have shown that global warming has exceeded 1.5 °C over the last 300 years. Increasing global temperatures impact multiple sectors, including environmental, agricultural, economic, health, social, technological, and political aspects [4]. The rise in global temperature has led to accelerated ice melting in Greenland and Antarctica [5], which has significantly contributed to sea-level rise, resulting in more frequent coastal floods. In addition, higher temperatures can reduce crop yields, alter growing seasons, and increase pest populations, thereby affecting both major food crops (rice, maize, wheat, etc.) and livestock through increased exposure to insects, parasites, and disease vectors [6–8]. Furthermore, heat can lower worker productivity, especially in outdoor industries like construction and agriculture [9]. Consequently, the risk of heatstroke and dehydration rises. Beyond these impacts, warmer climates can expand the range of vector-borne diseases like malaria and dengue fever [10]. These interconnected challenges underscore the growing need to develop new technologies to combat and adapt to a changing climate. This includes expanding the use of renewable energy sources and enhancing water resource management systems [11].

Governments worldwide have increasingly implemented policies to address climate change, impacting international relations and national strategies [12]. The Intergovernmental Panel on Climate Change (IPCC), established in 1988 by the World Meteorological Organization and the United Nations Environment Programme, is a United Nations body that provides policymakers with periodic, evidence-based scientific assessments on climate change, its implications, potential future risks, and proposes adaptation and mitigation strategies [13]. The relationship between global temperature and greenhouse gas concentrations is a crucial area of study in understanding climate change and associated factors. Over the past century, the earth's climate has undergone significant changes, largely attributed to anthropogenic activities that have increased the concentration of greenhouse gases in the atmosphere [14].

The greenhouse effect is essential for maintaining Earth's

habitable average surface temperature of approximately 15 °C, instead of −18 °C [15]. However, human activities have intensified this natural process, leading to accelerated global warming [16]. Fossil fuel combustion, deforestation, industrial production, waste management, and agricultural practices contribute substantially to atmospheric carbon dioxide (CO_2), methane (CH_4), nitrous oxide (NO_x), and fluorinated gases [17–19]. Atmospheric CO_2 has increased from 280 ppm to over 400 ppm since the Industrial Revolution [20]. Consequently, reducing greenhouse gas emissions remains an urgent global priority, supported by both mitigation strategies and emerging technologies such as CO_2 utilization through electrochemical, photocatalytic, and catalytic processes [21, 22].

However, alongside mitigation efforts, understanding and adapting to rising temperatures is equally critical. Ambient temperature is one of the most direct and measurable indicators of climate change, and accurate temperature prediction is essential for urban planning, public health preparedness, agricultural management, infrastructure protection, and disaster risk reduction. As global warming accelerates, cities-especially densely populated and climate-vulnerable regions-require reliable forecasting systems to anticipate temperature variations and implement early adaptation strategies.

Predicting ambient temperature trends is challenging due to the nonlinear nature of atmospheric dynamics and the complex interactions between greenhouse gases and other environmental variables. Traditional statistical models often fail to capture these intricate relationships, creating a growing need for advanced computational approaches. Artificial intelligence has emerged as a powerful tool for addressing such complexities [23, 24]. Machine learning, a subset of artificial intelligence, develops predictive models based on learning patterns from data without requiring explicit programming [25]. With increasing computational power and the availability of large datasets, machine learning has transformed numerous fields such as agriculture, healthcare, environmental science, and climate modeling [26, 27]. Environmental applications include predicting air particulate matter [28], forecasting water availability [29], modeling wastewater treatment systems [30], identifying pollutants [31], and optimizing renewable energy systems [32, 33].

In the context of climate research, machine learning has demonstrated strong predictive capability for ambient temperature estimation across different regions. For example, Fister *et al.* [34] predicted long-term air temperatures in Paris using multiple ML models, while Nematchoua *et al.* [35] predicted solar radiation and temperature across 27 European countries. Ding *et al.* [36] generated highly accurate air temperature maps for Guangzhou, China, and Wang *et al.* [37] reviewed over 900 studies, highlighting the substantial potential of ML for temperature prediction. Furthermore, several studies have explored ambient temperature prediction through mobile and web-based applications. For example, Aguilera *et al.* [38] employed weather data and basic building descriptors within a decision tree model to predict indoor air temperature and subsequently developed a user-friendly mobile application that reported an accuracy of 92%. Soyemi and Adesola [39] developed a decision-support framework aimed at improving agricultural productivity by providing farmers with accessible weather and agricultural guidance. The system, delivered through a web-based application supported by SMS technology, offers timely weather forecasts, agricultural advisories, and decision-making support tailored to farmers' needs, particularly in rural areas. Similarly, a web-based system employing a Fuzzy Time Series-Markov model achieved high accuracy in predicting air temperature and Relative Humidity (RH) using wireless sensors and real-time data transfer ($R = 0.9987$ for temperature; $R = 0.9946$ for humidity) [40].

Despite global advancements, Sri Lanka-and particularly Battaramulla region-lacks a comprehensive machine learning-based ambient temperature prediction framework that integrates greenhouse gases with other climatic factors. Previous attempts, such as Perera and Rathnayake [41], used limited variables due to data constraints and relied on basic ANN models. As a climate-sensitive city, Battaramulla urgently requires a robust, data-driven temperature prediction system to support public health, urban planning, agriculture, and disaster management. Therefore, this study aims to develop an explainable machine learning model capable of predicting ambient temperature in Battaramulla by incorporating greenhouse gases and other key environmental parameters. By leveraging explainable AI techniques, the model not only enhances predictive accuracy but also provides transparency into the relative importance of each climatic factor, offering valuable insights for policymakers and climate scientists.

To ensure transparency and interpretability of the proposed model, the study incorporates multiple explainable AI techniques. These include SHapley Additive exPlanations (SHAP), which quantify the contribution of each input feature to the model's output, Individual Conditional Expectation (ICE), which visualize the influence of a single feature across individual predictions, Partial Dependence (PDP), which show the average marginal effect of a feature on the predicted temperature, and Accumulated Local Effects (ALE), which show the effect of a feature on the predicted temperature while accounting for correlations with other features. Together, these methods provide both global and local interpretability, enabling stakeholders to understand not just the accuracy of predictions but also the rationale behind them an essential aspect for informed climate-related decision-making.

II. Materials and Methods

A. Machine Learning Algorithms

1) K-Nearest Neighbors (KNN)

KNN is widely used for pattern recognition and data mining studies [42]. This algorithm belongs to the category of lazy learning, as it stores all existing cases and determines new cases based on distance function criteria. The N dimensions represent vectors corresponding to each feature. The value of K is determined during the operation of the algorithm based on a set of objects with similar properties or values, which constitute the training dataset. K represents the number of elements considered when evaluating a new value. The distance between the new value and the existing elements

is calculated, and the new value is assigned to its nearest neighbor. Euclidean distance is commonly used as a similar metric for decision-making.

2) Decision Tree (DT)

The Decision Tree (DT) algorithm is a tree-based structure containing several branches and leaf nodes. Each branch represents a choice between different options, and each leaf node shows a specific classification or decision. The final tree outlines all possible scenarios, with each branch showing a decision and its outcome. This learning approach of the algorithm is used to approximate target functions with discrete values, representing the function and generating multiple branches and leaf nodes through recursive binary partitioning of the instance space [43]. At each node, the data is split based on criteria defined by tree-building algorithms such as Iterative Dichotomizer 3 (ID3) [44], Classification and Regression Tree (CART), and Chi-squared Automatic Interaction Detector (CHAID) [45].

3) Random Forest (RF)

The RF algorithm was introduced to reduce the overfitting of decision trees [46]. This algorithm is used for unpruned classification and regression and randomly selects training data for this mechanism. The RF trees are designed in parallel, and the Bagging (Bootstrap Aggregating) algorithm is used for the prediction [47]. The bootstrap sampling and aggregation of individual predictions are two key processes of Bagging. The sampling process produces data subsets for training the weak learners using sampling with replacement. The aggregation process is made as the average of the prediction of weak learners to decide the RF output. Apart from Bagging, RF incorporates a randomized feature selection process at the nodes to mitigate the correlation between the weak learners [48]. Hence, this process reduces the similarity of weak learners.

4) Support Vector Regression (SVR)

SVR algorithm is used for regression tasks and is an adaptation of the Support Vector Machine (SVM) algorithm, which is primarily used for classification [49]. Regression problems can be considered a generalization of classification. The SVM algorithm performs well in binary classification by formulating the problem into a convex optimization task [50]. The goal is to identify the hyperplane that maximizes the margin between classes while minimizing classification errors. The SVM algorithm achieves this optimal hyperplane by focusing on support vectors. Due to their sparse solutions and strong generalization capabilities, the SVM algorithm is extended to regression problems. Therefore, SVM is generalized as SVR by introducing an ϵ-insensitive region around the function, called the ϵ-tube. The regression models aim to predict continuous values. The regression model aims to estimate a continuous-valued function that maps input variables to a numerical output [51].

5) Histogram-based Gradient Boosting Regressors (HGBR)

HGBR algorithm is an enhanced version of the Gradient Boosting Regression Tree (GBRT) algorithm, utilizing histograms to improve computational efficiency and scalability [52, 53]. The fundamental approach of the HGBR algorithm involves discretizing continuous floating-point eigenvalues into integer-valued bins and setting up a histogram with the bin width of k. During data traversal, the histogram accumulates statistics based on the discretized indices values. After passing the data once, the histogram accumulates the necessary statistics. Then, subsequently, it efficiently traverses the discrete values of the histogram to identify the optimal split point and construct the gradient boosting tree. This approach significantly reduces the number of potential split points compared to sorting continuous values. Consequently, HGBR exhibits several advantages, including reduced memory consumption, faster computation, improved cache utilization, and a straightforward construction process. Hence, this is achieved through a histogram-based approach, similar to the iterative processes found in algorithms like XGBoost and LightGBM [53]. Thus, HGBR is particularly well-suited for regression tasks and is widely applied in fields such as agriculture and environmental science, particularly for high-dimensional data or datasets with mixed feature types.

B. Case Study and Data Collection

Colombo, Sri Lanka is significantly impacted by its air pollution levels and the temperatures are in the rising phase. Therefore, as discussed in the introduction, the Battaramulla area in Colombo was selected as the case study area. This was also due to the maximum availability of data. The hourly data on Carbon dioxide concentration (CO_2), Nitrous Oxide concentration (NOx), Ozone concentration (O_3) , Carbon Monoxide concentration (CO), Particulate Matter (with diameter $\leq$ 2.5 µm) concentration ($PM_{2.5}$), and Particulate Matter (with diameter $\leq$ 10 µm) concentration (PM_{10}) , ambient temperatures, relative humidity (RH), solar radiation, and rain gauge for Battaramulla were collected through the Central Environmental Authority in Sri Lanka (Fig. 1). The hourly wind speed for the Battaramulla area was obtained from the National Aeronautics and Space Administration (NASA) (refer the following website: https://power.larc.nasa.gov/data-access-viewer/). In addition, Methane concentration (CH_4) levels were collected from NASA due to the unavailability of ground measured data. Due to limited methane data and minimal differences between day and night concentrations, the average of day and night values was used to represent the hourly mean methane concentration across the entire day. The model was developed under data scarcity and arranged for April, July, August, and September in 2023.

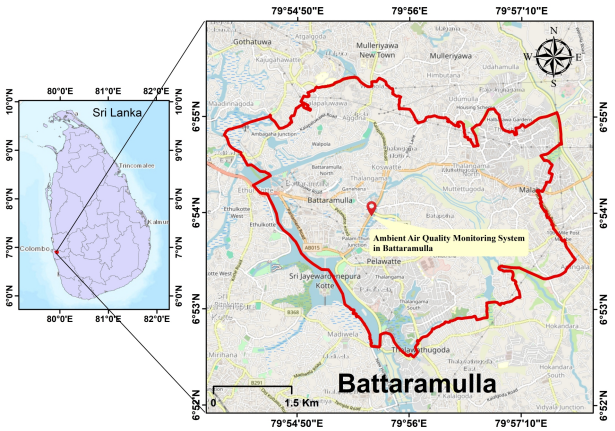

Fig. 1. The location of the ambient air quality monitoring system in Battaramulla, Sri Lanka.

C. Pre-processing

The raw meteorological and air quality data were pre-processed to enhance data quality and ensure suitability for machine learning analysis. Temporal variables, such as month, day, and hour, were converted into numerical format. The minimal missing data (<2%) were handled using linear interpolation based on nearby historical values, while statistical threshold based filtering was applied to reduce noisy observations and extreme outliers.

The processed dataset was split into 70% training, 20% testing, and 10% validation sets, with the split performed by including every study month to ensure reliable model evaluation and generalization. Moreover, the dataset was structured for model training with selected study months, in which past observations were used to predict future ambient temperature.

D. Model Development

According to the literature, there are many environmental factors directly associated with ambient temperature. Relative humidity [54], solar radiation [55], rainfall [56], wind speed [57], CO_2 concentration [58], NO_x concentration [59], CH_4 concentration [60], O_3 concentration [61], CO concentration [62], $PM_{2.5}$, and PM_{10} [63] directly impact the ambient temperature. The mathematical formulation for the prediction model is given in Eq. (1).

According to the raw dataset, the temperature deviation is shown in Fig. 2. The trend indicates that the month of April exhibits greater fluctuations than the other months, with generally higher temperature values.

$$Ambient\ Temperature = \Phi\left(\begin{array}{c}\text{Relative humidity, solar radiation,}\\ \text{rain gauge,}\\ \text{wind speed, } CO_2 \text{ concentration,}\\ NO_x \text{ concentration, methane concentration,}\\ O_3 \text{ concentration, CO concentration,}\\ PM_{2.5}, PM_{10}, \text{Month, Day, Hour}\end{array}\right) \quad (1)$$

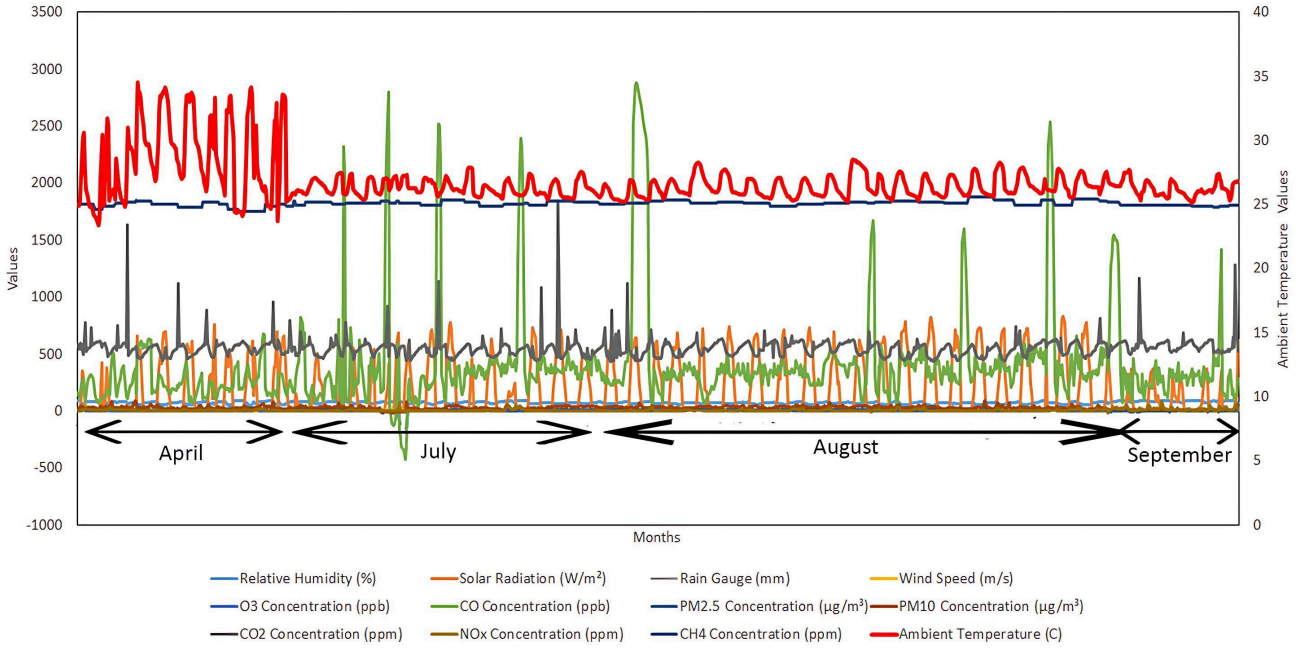

Fig. 2. Temporal trend plot of raw dataset.

Five machine learning algorithms were used to develop the prediction model based on Eq. (1). They are K-Nearest Neighbors (KNN), Decision Tree (DT), Random Forest (RF), Support Vector Regression (SVR), and Histogram-based Gradient Boosting Regressor (HGBR).

The KNN model was developed with k = 10, and for the training dataset, the accuracy evaluation metrics demonstrated the algorithm's ability to capture hidden patterns. In the DT algorithm, the most suitable values for the hyperparameters, including the maximum depth of the tree, the minimum number of samples required to split an internal node, the minimum number of data samples at a leaf node, and the maximum number of leaf nodes, were determined using the grid search method from scikit-learn. The optimal values were 5, 2, 1, and 50, respectively. In the RF algorithm, hyperparameters such as the number of weak learners = 100, maximum depth of each tree = 30, minimum sample splits = 5, features for each split = 0.7, and minimum samples per leaf nodes = 3 were applied. In SVR, the power transformation with the Yeo-Johnson method was applied to preprocess the data. This is to ensure a stable variance and an approximate Gaussian distribution. Both the training and testing features were scaled using this transformation. In addition, this algorithm was configured with optimal hyperparameters as follows: the regularization parameter was set to 6.0, the epsilon (ε) was defined as 0.1, and the gamma (γ) was set to 0.01. The Radial Basis Function (RBF) kernel was used because it is particularly effective at capturing non-linear relationships in the data, making it well-suited for complex regression tasks. The following hyperparameters to balance performance and efficiency were used in the HGBR algorithm. The learning rate was set to 0.05, and a total of 300

iterations were specified to allow a sufficient training process, and the maximum number of leaf nodes was set to 20 to ensure controlling overfitting. The minimum number of samples per leaf was 5, and slight L2 regularization with a value of 0.1 was applied.

E. Application of Explainable Machine Learning

Explainable machine learning techniques were considered in this research to increase model trust and examine the effect of features on predictions. Methods such as SHAP, PDP, ICE, and ALE were utilized to provide deeper insights into the model's predictions and the influence of various features on the outcomes.

1) SHapley Additive exPlanations (SHAP)

SHAP explainable method is an advanced interpretability method used in machine learning to explain the predictions of complex models by assigning contributions to individual features. Hence, the main idea behind SHAP is to allow for a clear understanding of the influence of each feature on the model outcomes with SHAP values. The Shapley values ensure that the contributions are distributed relatively based on the marginal contribution of features across all possible subsets. A unique aspect of SHAP is its flexibility in defining the "players". For tabular data, individual feature values can serve as players, while for other types of data, such as images, players can be grouped into meaningful clusters, like superpixels, to explain the prediction. An important innovation of SHAP is its representation as an additive feature attribution method. This means the Shapley value explanation is expressed as a linear model, where the prediction is broken down into the sum of the contributions of all features. This additive structure makes SHAP explanations intuitive, consistent, and directly comparable across features. SHAP has become a powerful tool for understanding machine learning models, particularly in identifying key drivers of predictions, revealing feature interactions, and improving the transparency and trustworthiness of black-box models [64, 65].

2) Partial Dependence Plot (PDP) and Individual Conditional Expectation (ICE) plots

The Partial Dependence Plot (PDP) [66, 67] and Individual Conditional Expectation (ICE) [68, 69] methods are complementary visualization techniques used in machine learning to display the relationship between features and model predictions. The PDP provides a global perspective by illustrating the average relationship between one or more features with the predicted outcome. It helps in understanding how a feature affects the prediction values across the entire dataset, making it particularly useful for interpreting complex models.

In addition, ICE plots offer a more granular, instance-specific perspective. This method shows how the model prediction for an individual instance changes as the value of a specific feature varies while keeping all other features constant. Each instance is represented by a separate line, highlighting the unique, instance-specific relationship between the feature and the predictions. Together, PDP and ICE plots provide both global and local insights into feature effects. PDPs give an overall view of the average impact, while ICE plots show heterogeneity and interactions that might be obscured in the average trends of PDPs. This combination is a powerful tool for understanding and interpreting machine learning models. Therefore, this study discusses the use of the PDP explainability method to analyze two factors theoretically deemed most influential, two factors theoretically considered least influential, two factors identified as having the most significant impact during the model training stage, and two factors with the least impact according to the model training stage. The ICE plots were generated to examine the variation in predictions across 100 instances for each of the five most impactful factors, while all other factors were held constant [70].

3) Accumulated Local Effects (ALE)

ALE method is model-agnostic interpretability technique developed to explain predictions generated by complex black-box machine learning models. This method quantifies the local changes in model predictions within small intervals of a feature, allowing the overall marginal effect of each predictor to be visualized while reducing bias caused by correlated variables in the dataset [71]. Compared with commonly used interpretation tools such as PDP and SHAP, ALE provides a more reliable functional decomposition of model behaviour and is computationally efficient for analysing feature effects [72]. Nevertheless, several challenges remain in interpretable machine learning when applying ALE, including concerns regarding the reliability of results derived from bootstrapping procedures, particularly for small datasets where conventional training–test splitting may be limited [73]. Furthermore, determining meaningful effect sizes for individual predictors and making statistically reliable inferences from machine learning outputs remain active research areas in model interpretability [72]. Despite these limitations, ALE remains a powerful visual tool for characterizing the relationships between predictors and outcomes across a wide range of machine learning models.

F. Model Accuracy Evaluation

Widely used Mean Squared Error (MSE) and the coefficient of determination (R^2) were used as the performance evaluating matrices for the developed models. Low MSE values and high R^2 values (closer to 1) showcase the better performance of the predicted models.

The MSE is defined as the average of the squared differences between predicted and actual values. A lower MSE indicates a model with better predictive performance. Mathematically, MSE is given by Eq. (2).

$$\mathrm{MSE} = \frac{1}{\mathrm{n}}\sum_{\mathrm{i}=1}^{\mathrm{n}}(\mathrm{y_i} - \hat{\mathrm{y}}_\mathrm{i})^2 \tag{2}$$

where y_i is the actual value, $\hat{y}_i$ is the predicted value, and n is the number of observations. MSE penalizes larger errors more significantly due to the squaring term, making it sensitive to outliers [74, 75].

R^2, also known as the coefficient of determination, explains the proportion of the variance in the dependent variable that is predictable from the independent variables. It is calculated as Eq. (3).

$$\mathrm{R}^2 = 1 - \frac{\sum_{\mathrm{i}=1}^{\mathrm{n}}(\mathrm{y_i}-\hat{\mathrm{y}}_\mathrm{i})^2}{\sum_{\mathrm{i}=1}^{\mathrm{n}}(\mathrm{y_i}-\bar{\mathrm{y}})^2} \tag{3}$$

where $\bar{y}$ is the mean of the actual values. An R^2 value of 1 indicates perfect prediction, whereas a value closer to 0 indicates poor prediction. R^2 helps in interpreting how well the model generalizes to unseen data and is particularly useful when comparing different models on the same dataset [75, 76].

G. Development of Web Application and Overall Methodology

A web application based on the prediction models was developed as a user-friendly interface. This application allows users to input 14 environmental parameters: month, day, hour, relative humidity (%), solar radiation (W/m²), rainfall (mm), wind speed (m/s), CO_2 concentration (ppm), NO_x concentration (ppm), CH_4 concentration (ppm), O_3 concentration (ppb), CO concentration (ppb), $PM_{2.5}$ concentration (µg/m³), and PM_{10} concentration (µg/m³). When applying the month feature, it is limited to accepting only values from four months: April, July, August, and September.

The overall methodology carried out in this research is illustrated in Fig. 3.

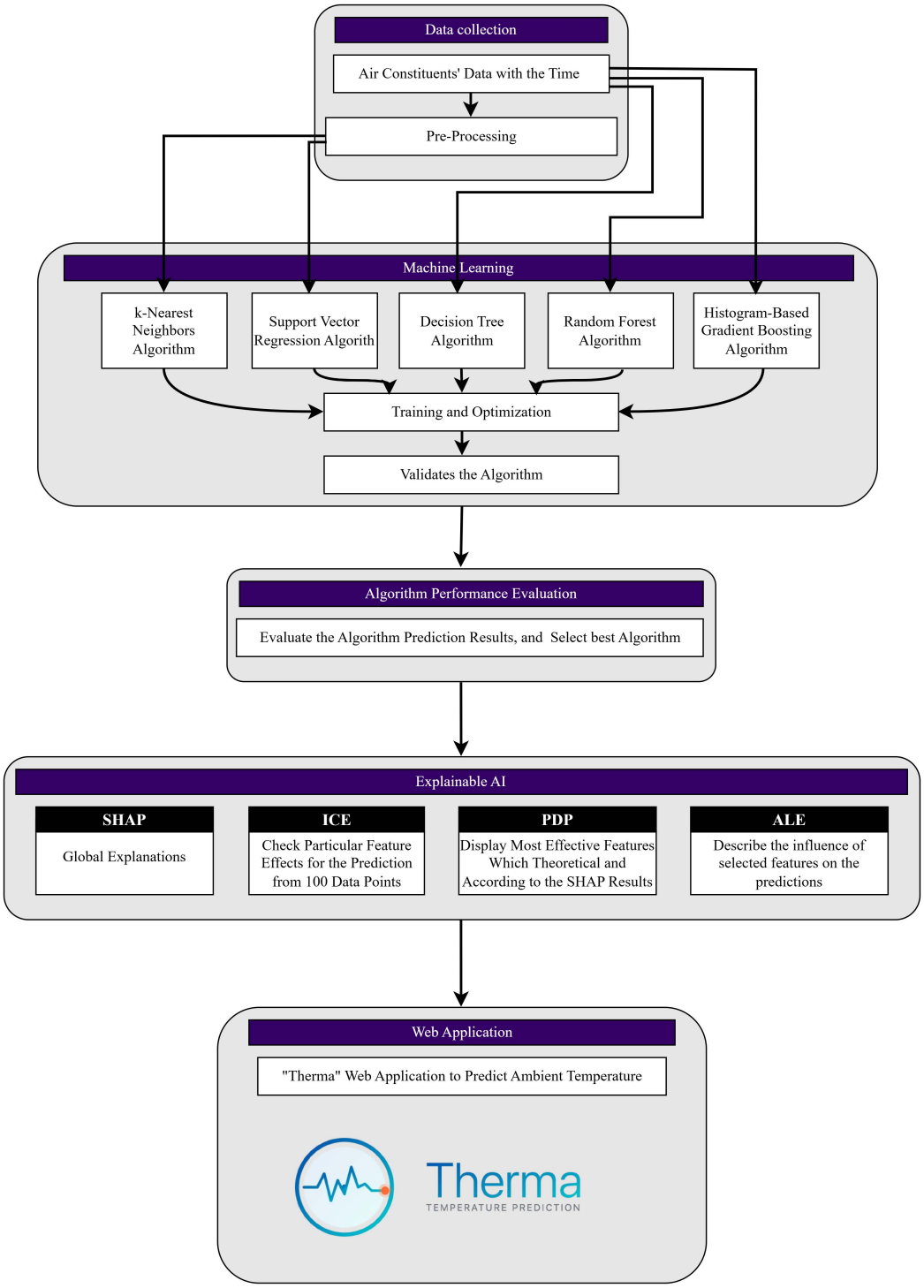

Fig. 3. Overall methodology.

III. Results and Discussion

A. Performance of Developed Prediction Models

Table 1 showcases the coefficient of determination between the predicted ambient temperature and measured temperature. The results demonstrated that the HGBR algorithm significantly outperformed other models in the training and testing stages, recording R^2 values of 1 and 0.96, respectively. In contrast, the SVR model exhibited the lowest performance, with R^2 values of 0.87 during training and 0.86 during testing. Nevertheless, SVR showcases a very good performance. These findings highlight the superior predictive accuracy and reliability of the HGBR model, making it a more robust choice for this application. The results emphasize the potential of the HGBR model in capturing the underlying relationships in the data, as opposed to the less effective predictions observed with the SVR model.

In addition, the MSE quantifies the average squared difference between predicted values and actual values, with lower values indicating better model performance. In this case, the HGBR model outperformed all other models, achieving the lowest MSE values for both the training and testing stages. Specifically, the HGBR model recorded an MSE of 0.01 during the training phase and 0.11 during testing, signifying a highly accurate fit with minimal prediction error. Moreover, the Mean Absolute Error (MAE) [75] achieved the lowest values of 0.03 and 0.21 in the training and testing stages, respectively. Furthermore, the RMSE also depicted the lowest values of 0.05 in the training stage and 0.34 in the testing stage, in contrast to other models.

Table 1. Training and testing R^2 and MSE, RMSE, and MAE values across different models

Model	R^2		MSE		RMSE		MAE	
	Training	Testing	Training	Testing	Training	Testing	Training	Testing
DT	0.95	0.90	0.15	0.26	0.39	0.51	0.29	0.37
HGBR	**1.0**	**0.96**	**0.01**	**0.11**	**0.05**	**0.34**	**0.03**	**0.21**
KNN	0.9	0.88	0.29	0.32	0.54	0.57	0.39	0.41
RF	0.99	0.93	0.05	0.19	0.22	0.44	0.15	0.30
SVR	0.87	0.86	0.38	0.37	0.62	0.61	0.44	0.45

Conversely, the SVR model demonstrated the highest MSE values among the tested models, with 0.38 for training and 0.37 for testing. This indicates that SVR had relatively larger prediction errors and was less effective at capturing the underlying patterns in the data compared to HGBR. The results underscore the superior predictive capability of the HGBR model, which exhibited remarkable consistency between training and testing, pointing to its robustness and generalizability. In contrast, the higher MSE values observed for SVR suggest limited effectiveness in reducing error, particularly when compared to HGBR. These findings highlight the HGBR model as a reliable choice for achieving high accuracy and minimal error in predictive modeling tasks. Graphical representation of the performance of the models is shown in Fig. 4.

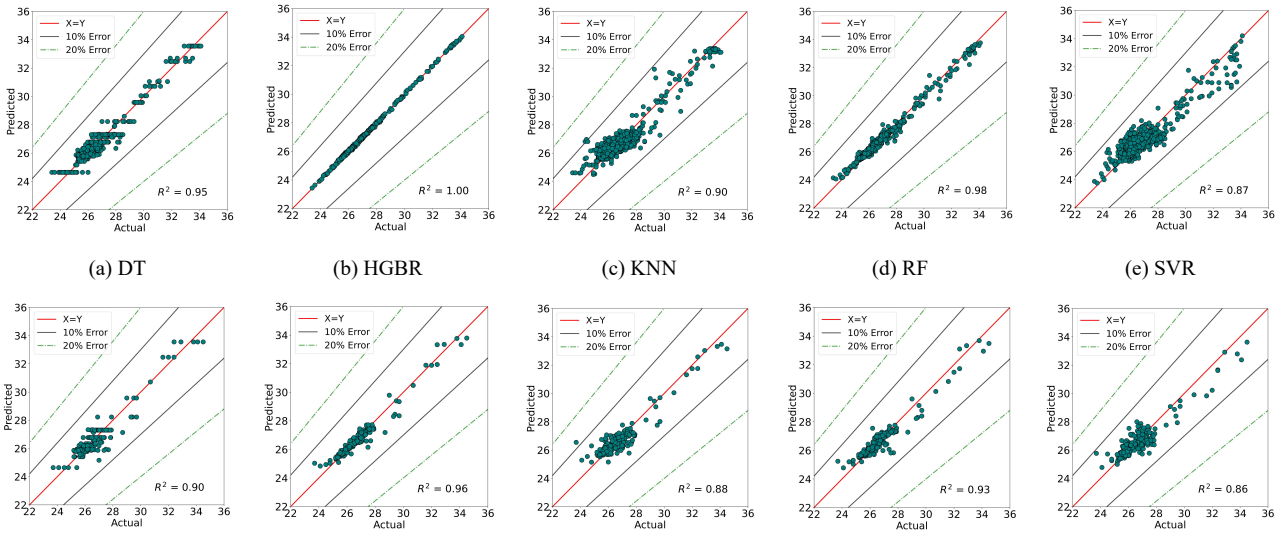

(a) DT (b) HGBR (c) KNN (d) RF (e) SVR

(f) DT (g) HGBR (h) KNN (i) RF (j) SVR

Fig. 4. Comparison of actual and predicted values with different Models. (a) to (e) denote the training results of the models, while (f) to (j) denote the testing results of the models. (Units of X and Y axes are in °C).

B. Evaluating HGBR Model Uncertainty Across the Test Samples

Fig. 5 presents the model predictions for the first 100 test samples, sorted in ascending order by the observed target value. The blue line with circular markers represents the actual observed values, while the red line with square markers shows the corresponding model predictions. The shaded region denotes the 80% prediction interval, reflecting the model's estimated uncertainty around each prediction.

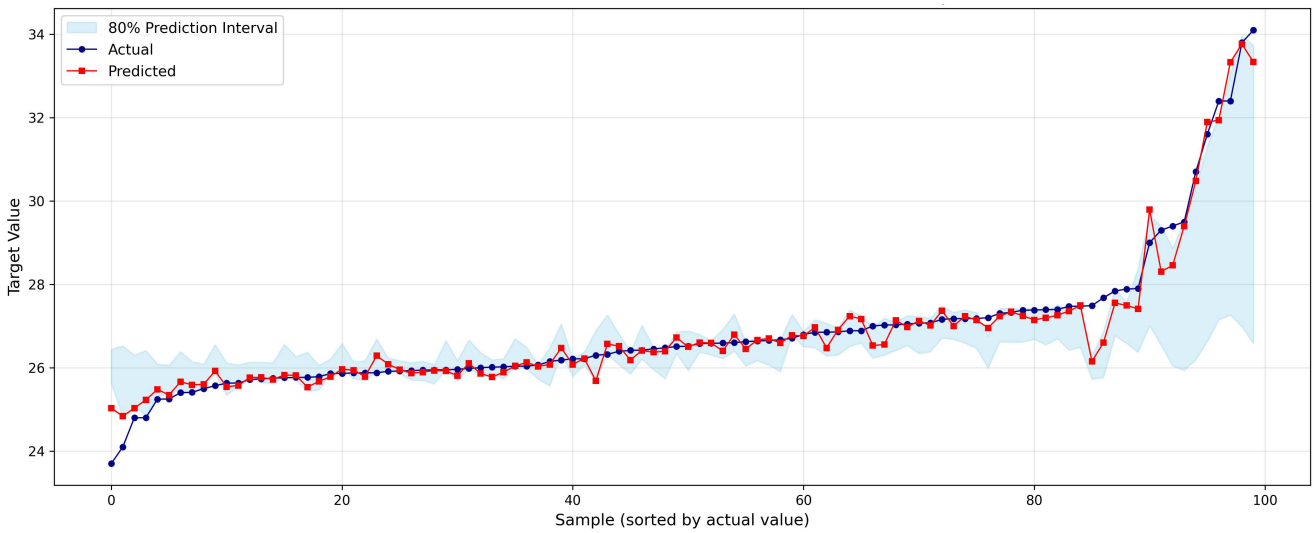

Fig. 5. Prediction with 80% prediction intervals for the first 100 test samples.

Across most of the lower and mid-range values, the predicted series closely follows the observed trend, indicating strong agreement between predicted and actual values. In this range, the majority of observed points lie within the 80% prediction intervals, suggesting that the uncertainty estimates are reasonably well calibrated. The relatively narrow width of the prediction intervals in this region indicates higher model confidence under more stable conditions.

As the target values increase toward the upper end of the distribution, greater variability between predictions and observations is observed, accompanied by a noticeable widening of the prediction intervals. This behaviour indicates increased predictive uncertainty at higher values. Despite this, the prediction intervals continue to capture most of the observed values, demonstrating that the model appropriately expands its uncertainty bounds under more challenging conditions.

The scatter plot in Fig. 6 presents predicted values against observed values, together with the 1:1 reference line representing perfect agreement between predictions and observations. Most data points lie close to this line, indicating strong agreement and good predictive performance across the observed range. The vertical error bars represent the 80% prediction intervals, which quantify the model's uncertainty for each prediction. These intervals generally encompass the observed values, demonstrating reasonable uncertainty calibration.

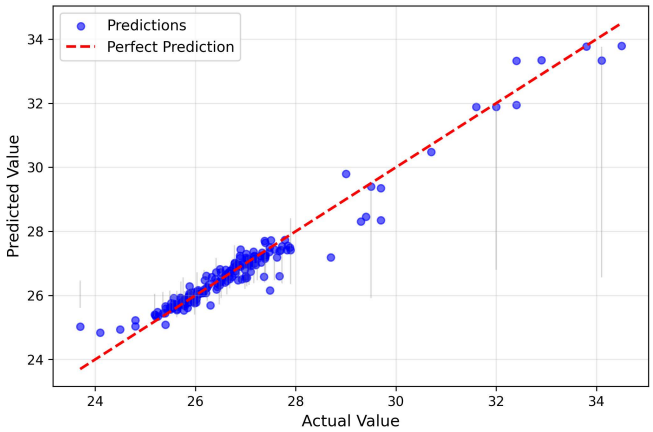

Fig. 6. Actual vs Predicted with 80% prediction intervals.

A slight widening of the prediction intervals is observed at higher values, suggesting increased uncertainty under more extreme conditions. Nevertheless, the majority of predictions remain close to the ideal line, confirming that the model captures the underlying relationship effectively while providing meaningful uncertainty estimates.

C. *Distribution of HGBR Model Prediction Errors*

The Fig. 7 illustrates the distribution of prediction errors (predicted-observed values) for the model. The error histogram is approximately symmetric and centred close to zero, as indicated by the dashed vertical line, suggesting that the model does not exhibit a strong systematic bias toward over- or under-prediction. Most errors are concentrated within a narrow range around zero, indicating generally high prediction accuracy for the majority of observations. A small number of larger positive and negative errors are present in the tails of the distribution, reflecting occasional deviations under more extreme conditions. Overall, the error distribution suggests stable model performance with limited dispersion and acceptable residual behaviour.

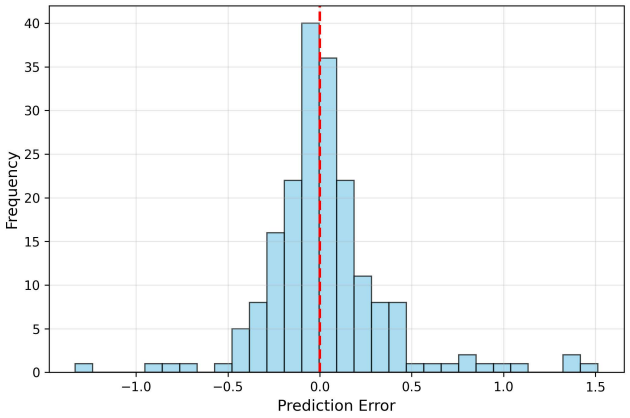

Fig. 7. Distribution of prediction errors.

D. *SHAP Based Feature Contribution Analysis*

As per the above results, the prediction model developed based on the HGBR algorithm was selected for further analysis. Fig. 8 showcases the SHAP summary plot, providing an overall picture of how each feature contributes to the output of the HGBR algorithm. The X-axis of the plot showcases the impact of each feature on model prediction.

Positive values push prediction higher while negative values lower the prediction. The Y axis presents the features by their rankings. The color gradient, transitioning from blue to yellow, represents the progression of feature values from low to high, illustrating their varying impact. Results revealed that solar radiation, month and hour have strong impact in the prediction. Month and hour are the temporal variations; therefore, this showcases daily and seasonal variations. The wider SHAP value ranges showcase the strong influence in predictions. Hours (mid-day) tend to influence the temperature as expected due to increased solar activity. In addition, summer months have higher influence on the predictions. These features can be clearly visible from the SHAP plot.

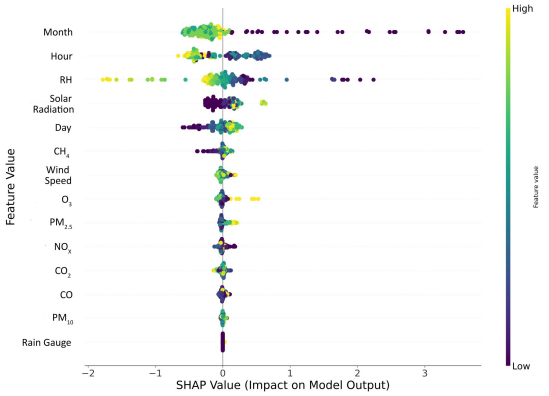

Fig. 8. SHAP values for the different features used in the HGBR model.

In addition, solar radiation has a significant influence on the predictions. Solar radiation influences atmospheric chemical reactions. This can lead to the formation of O_3. Higher positive SHAP values suggest that stronger sunlight leads to higher ambient temperatures as expected. Furthermore, relative humidity has a minor impact on the model prediction. It has some higher SHAP values but with lower feature values. It also has some positive and negative mixed SHAP values. Therefore, relative humidity interacts with other features. As expected, wind speed has some negative impacts. It helps to disperse pollutants in the environment and negatively impact the temperature predictions. However, most of the strong points are closer to zero. The SHAP values for pollutants are aligned near zero suggesting there is no major influence.

E. ICE Based Feature Contribution Analysis

A similar analysis was carried out on the model based on the KNN algorithm too. Based on the SHAP values of both HGBR and KNN, features such as Month, Hour, Relative Humidity, Solar Radiation, and Day had a more significant impact than other factors for both models. Fig. 9 presents ICE plots for these factors. Panels (a) to (e) show the results for the HGBR model, while panels (f) to (j) display the results for the KNN algorithm.

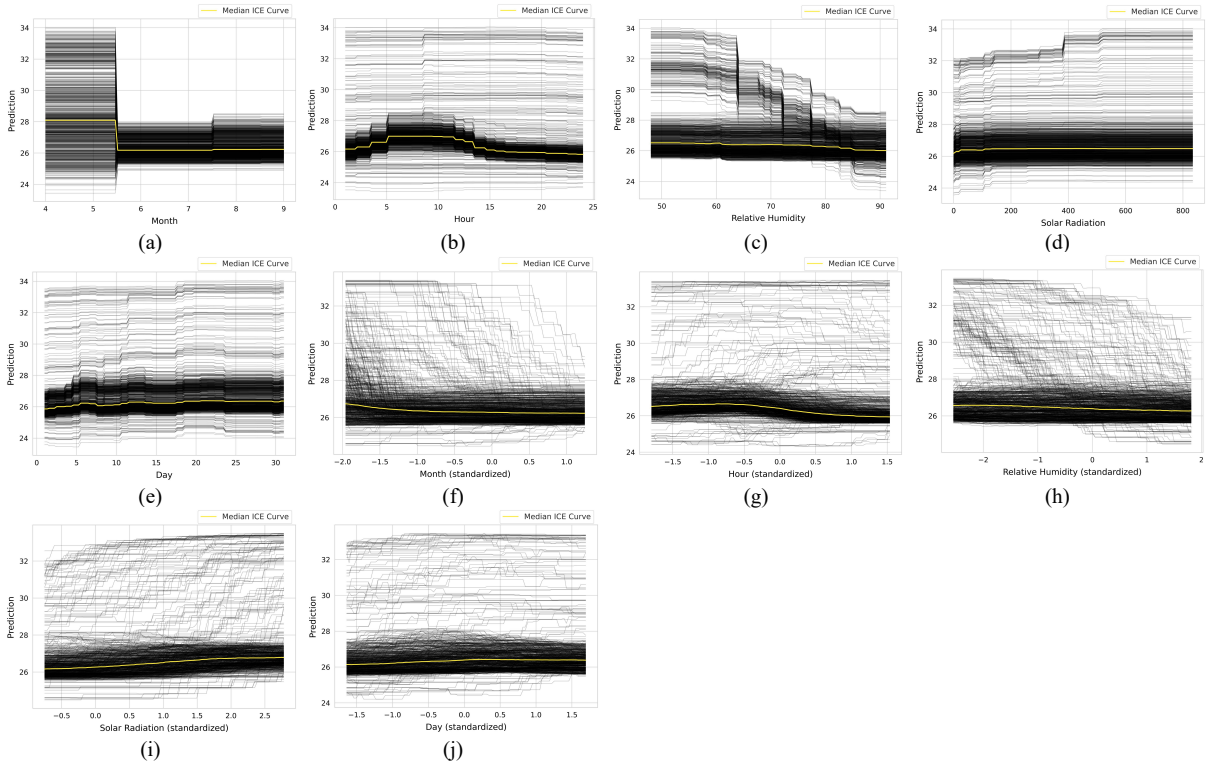

Fig. 9. ICE plots of HGBR and KNN models. Plots (a)–(e) represent the HGBR model, and plots (f)–(j) represent the KNN model for the factors month, hour, relative humidity, solar radiation, and day, respectively.

The Fig. 9(a) and (b) plots provide insights into how the Month and Hour features impact the prediction values of the HGBR model. For Month, the predicted values (ambient temperature) remain consistent for specific intervals but exhibit noticeable shifts at certain points, particularly around the transition from one month to another. Similarly, the Hour feature demonstrates a dynamic effect on predictions throughout the day. The predictions increase during early hours, peak around specific times, and gradually decline as the day progresses. The plots Fig. 9(c)–(e) show the impact of the Relative Humidity, Solar Radiation, and Day features, respectively, on the prediction values of the HGBR

algorithm. For relative humidity, the prediction values generally decrease as humidity increases, but individual data points often behave differently indicating a complex impact. In addition, for solar radiation, the prediction values tend to increase with rising radiation levels, though many instances deviate from this trend, highlighting the diverse effects of this feature. Moreover, the plot of Fig. 9(e) related to the feature of 'day', the median ICE curve shows a slight increase in predictions with the end of the months, but individual patterns are complex. The impact of the standardized features, according to the median ICE curve of the plots related to the KNN algorithm, does not show significant changes with variations in feature values.

F. PDP Based Feature Contribution Analysis

Fig. 10 presents a series of PDP contour maps that illustrate the interactive effects of various factors on the HGBR model predictions. Contour map Fig. 10(a) focuses on the two most influential features identified by SHAP analysis, while map Fig. 10(b) examines the two least influential features. Similarly, plots Fig. 10(c) and (d) analyze the impact of the two most and least influential features, respectively, based on real-world scenarios.

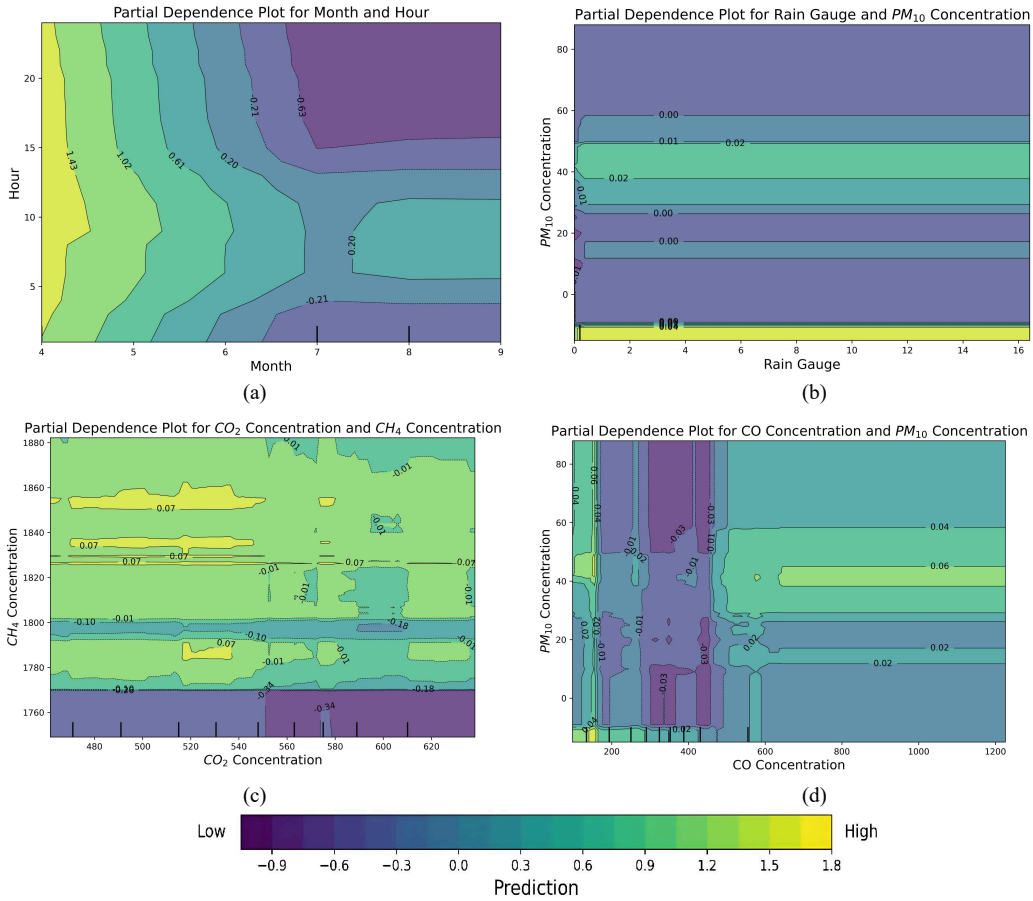

Fig. 10. PDP contour map of the most and minimum influential factors.

Contour map Fig. 10(a) represents the two most affected features according to the SHAP results for the HGBR algorithm's predictions. Contour map Fig. 10(b) represents the two least effected features according to the SHAP results for the HGBR algorithm's predictions. Contour map Fig.10(c) represents the two most effected features based on the real-world scenario for the HGBR algorithm's predictions. Contour map Fig. 10(d) represents the two least effected features based on the real-world scenario for the HGBR algorithm's predictions.

Fig. 10(a) map depicts the features 'hour' and 'month' that have a significant effect on the ambient temperature predictions of the HGBR algorithm. Hence, contour maps show a clear interaction between these two variables, with distinct color variations between the blue and yellow observed effect of hour and month combinations. For instance, certain hours during specific months demonstrate sharp gradients, highlighting the model sensitivity to seasonal and diurnal variations. This indicates that the dynamics captured by these features are crucial for accurately predicting ambient temperature, emphasizing their importance in the prediction process. In addition, according to Fig. 10(b), the 'PM_{10} concentration' and 'rain gauge' illustrate that these features have minimal influence on the model predictions. The uniform contour lines and spread of blue colors depict a weak dependency, with little interaction effect between these variables for predictions. The prediction stage of the HGBR algorithm remains largely consistent regardless of changes in PM_{10} levels and rain gauge measurements.

Fig. 10(c), 'CH_4 concentration' and 'CO_2 concentration,' illustrates the interaction effects of these two features on the model's predictions. This contour map highlights significant subtle dependencies, with certain ranges of CO_2 and CH_4 concentrations demonstrating moderate variations in the model output. For instance, low CO_2 and high CH_4

concentrations indicate a high prediction value, while low CH_4 and high CO_2 concentrations result in low prediction values for the algorithm. However, the overall contour patterns indicate relatively weak interactions, with prediction values remaining consistent across large areas of the feature space. Fig. 10(d) depicts the interaction effects between 'PM_{10} concentration' and 'CO concentration' for the model prediction values. According to the contour map, high PM_{10} and low CO concentrations indicate lower predicted values, while high levels of both PM_{10} and CO concentrations indicate significantly higher predicted values. Therefore, both CO and PM_{10} concentrations have considerably affected the model predictions.

G. ALE Based Feature Contribution Analysis

The one-dimensional Accumulated Local Effects (ALE) plots illustrate the marginal influence of notable patterns of six environmental variables on the predicted ambient temperature by the HGBR model, while accounting for feature interactions (Fig. 11). The shaded regions represent the 95% confidence intervals, while the rug plots indicate the distribution of observations used to compute the ALE estimates.

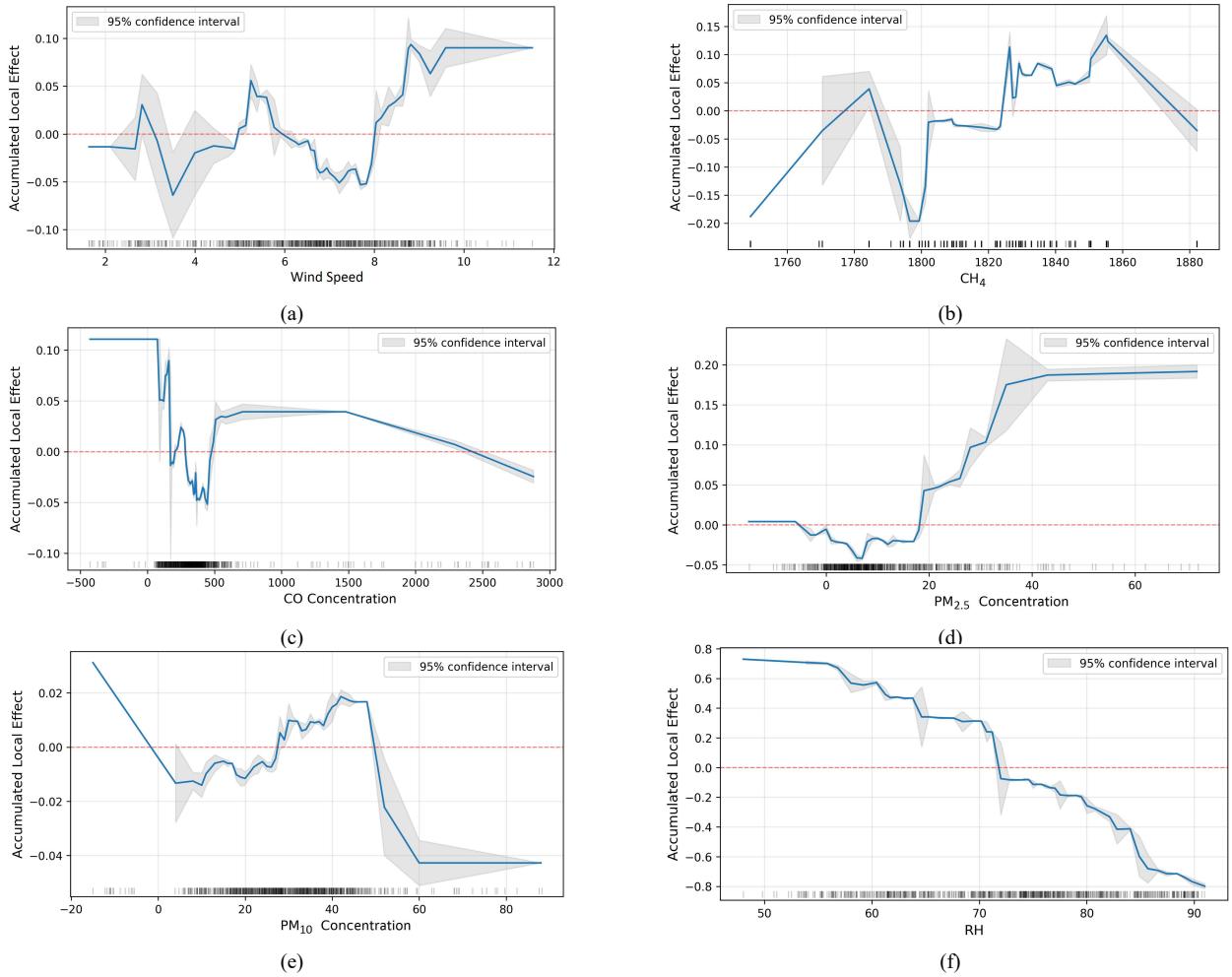

Fig. 11. ALE plots of the features. (a) Wind Speed, (b) CH_4, (c) CO Concentration, (d) $PM_{2.5}$ Concentration, (e) PM_{10} Concentration, (f) RH.

Wind speed exhibits a generally positive influence on temperature predictions at higher values (>8), indicating that stronger wind conditions tend to increase the predicted temperature contribution in the model. CH_4 shows a non-linear relationship, with temperature contributions considerably increasing around 1825–1855 ppm but declining at higher concentrations. CO demonstrates a moderate positive effect at lower concentrations (<1000 ppb), followed by a gradual decrease at higher concentrations.

Particulate matter variables show contrasting behaviors, where $PM_{2.5}$ displays a positive effect at higher concentrations (>20 μg/m³), while PM_{10} shows a slight positive influence at moderate levels followed by a negative effect beyond approximately 50 μg/m³.

The RH demonstrates a strong negative relationship, with higher humidity substantially reducing predicted temperature contributions.

H. Web Based Application

Fig. 12 presents the novel web-based application, 'Therma' developed based on the results of the study. This application allows users to input 14 environmental parameters: month (April, July, August, and September), day, hour, relative humidity (%), solar radiation (W/m²), rainfall (mm), wind speed (m/s), O_3 concentration (ppb), CO concentration (ppb), $PM_{2.5}$ concentration (μg/m³), PM_{10} concentration (μg/m³), CO_2 concentration (ppm), NO_x concentration (ppm), and CH_4 concentration (ppm). Once the user enters these values, the application utilizes the optimized HGBR algorithm to process the data in the back end, generating an accurate prediction of the ambient temperature in Battaramulla, Sri Lanka.

The web application is hosted within a cloud environment and made publicly accessible through a secure tunneling service. To achieve this, a tunnel is established to the private cloud environment via a specified port using the Ngrok executable process. This creates a publicly accessible, temporary URL that is then shared with end-users. When users access the web application through this URL, their requests are first routed to the Ngrok web server, since the URL falls under the ngrok.com subdomain. Ngrok then maps the incoming request to the corresponding application by linking it to the previously established tunnel. Finally, the request is forwarded through this tunnel to the hosted application, enabling seamless user access over the internet [77].

In the 'Therma' application, all features must be provided for the model to make accurate predictions. If any input feature is missing, the model cannot predict the ambient temperature and an error message will appear for the end user. This application aims to be a valuable resource for various stakeholders, including researchers, environmental agencies, and the general public, who require reliable temperature information for planning and decision-making.

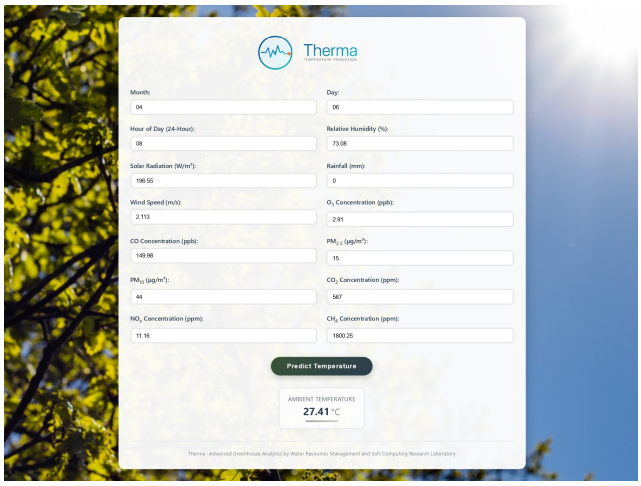

Fig. 12. Interface of the 'Therma' web application.

I. *Application validation*

The developed application validation process was conducted with new values and ambient temperature data. To assess the accuracy of the developed application, 192 points of real-time unseen data were used, equally distributed across four selected months in this study. After prediction, the differences between the actual and predicted values were analyzed (refer to Fig. 13). The blue dots represent the actual temperature measurements, while the red dots represent the corresponding temperature values predicted by the developed application. The application predicts the ambient temperature with minimal errors. As depicted in the plot, some predictions overestimate the temperature, while some predictions underestimate the actual values with a minor error. Moreover, these discrepancies mentioned the presence of noise in the data, but it has not significantly affected the HGBR training process according to the line graph.

The values demonstrated minimal deviations from the real-time data, indicating that the model performed with high accuracy and minimal errors. Hence, the overall plot is depicted that the application predictions align reasonably well with the actual temperature readings.

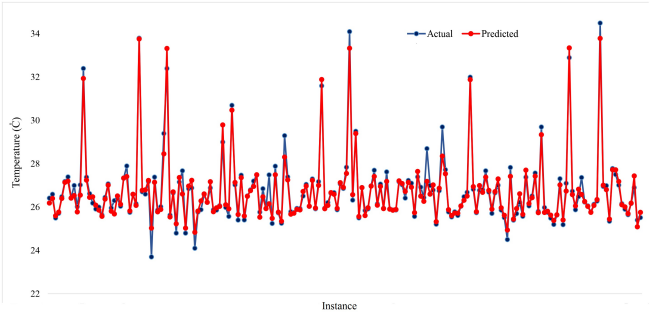

Fig. 13. Validation plot of the developed web application based on real-time data.

IV. Alignment to Sustainable Development Goals

Climate change directly impacts many of the Sustainable Development Goals (SDGs) and ambient temperature is one of the most important parameters in climate change. It is in the rising phase due to anthropogenic activities, and it is important to understand its significance in highly urbanized areas like capital cities. Ambient temperature has direct influences in SDG2: Zero Hunger, SDG6: Clean Water and Sanitation, SDG7: Affordable and Clean Energy, SDG11: Sustainable Cities and Communities, SDG13: Climate Action, SDG14: Life below Water and SDG15: Life on Land. In addition, this is a factor that interconnects all other SDGs. Therefore, accurate prediction of ambient temperatures is highly important in achieving SDGs for a meaningful future. Therefore, understanding its importance, this research showcases predicting one of the most important climatic parameters in a concerned area. The findings can be used to implement any adaptation strategies for climate change.

V. Conclusions

This research offers a comprehensive approach to predicting ambient temperature in Battaramulla division in Sri Lanka. The integration of advanced algorithms, such as HGBR and KNN, showed the higher coefficient of determination values and lowest MSE, RMSE, and MAE values of these tree-based and non-tree-based models. Explainable artificial intelligence-based SHAP values revealed that key features including Month, Hour, Relative Humidity, Solar Radiation, and Day exert the most significant influence on temperature fluctuations of both HGBR and KNN models. These findings underscore the value of data-driven insights for understanding complex environmental dynamics during the selected months. The development of the 'Therma' web application represents a pivotal step in operationalizing these insights. The ability of the application to process 14 environmental parameters and deliver precise real-time temperature predictions highlights its utility as a robust, user-centric tool for environmental monitoring.

Validation using 192 real-time data points demonstrated the exceptional accuracy of the model, with minimal prediction errors. Moreover, the incorporation of SHAP, PDP, ICE and ALE enabled a detailed interpretation of feature interactions, facilitating a nuanced understanding of their roles in temperature prediction. This study not only

establishes the effectiveness of machine learning in environmental modeling but also lays the groundwork for scalable and adaptable predictive frameworks. Despite these strengths, the framework exhibits several limitations. The requirement for multiple user-provided inputs may reduce usability, and the model is currently constrained by its spatial and temporal scope, having been trained exclusively for the Battaramulla region and limited months of 2023 due to data availability.

Future research should therefore emphasize time aware validation strategies to assess temporal stability, incorporate uncertainty quantification to support risk informed decision making, and integrate lagged and autoregressive features to better capture temporal dependencies in temperature dynamics. Expanding the spatial and temporal coverage to include diverse geographic regions, longer observation periods, and additional climatic variables would further enhance generalizability. Such advancements will strengthen the scalability and adaptability of the proposed framework, increasing its potential contribution to climate-sensitive planning, sustainable development, and evidence-based policy formulation.

Conflict of Interest

The authors declare no conflict of interest

Author Contributions

H.S. and T.A. investigation, methodology, modelling and programming, writing original draft; S.B. data processing, analysis, visualization; Y.A. visualization; N.R. validation and writing and reviewing; K.K. writing and reviewing; U.R. conceptualization, writing and reviewing, validation, supervision; all authors had approved the final version.

Data Availability Statement

Some of the data used in this paper are unavailable due to data purchases for another project (Forecasting air quality project, P142025).

Acknowledgments

We thank Ruchiru Dilshan for discussions on related topics and for cartographic support.

References

[1] S. A. Bandh, S. Shafi, M. Peerzada *et al.*, "Multidimensional analysis of global climate change: A review," *Environmental Science and Pollution Research*, vol. 28, no. 20, pp. 24872–24888, 2021. https://doi.org/10.1007/s11356-021-13139-7

[2] R. Ramesh and R. Purvaja, "Climate change and coastal ecosystems: An overview," *Asian Journal of Water, Environment and Pollution*, vol. 1, no. 1–2, pp. 29–40, 2004. https://doi.org/10.3233/AJW-2004-1_1-2_06

[3] M. T. McCulloch, A. Winter, C. E. Sherman *et al.*, "300 years of sclerosponge thermometry shows global warming has exceeded 1.5 °C," *Nature Climate Change*, vol. 14, no. 2, pp. 171–177, 2024. https://doi.org/10.1038/s41558-023-01919-7

[4] K. Abbass, M. Z. Qasim, H. Song *et al.*, "A review of the global climate change impacts, adaptation, and sustainable mitigation measures," *Environmental Science and Pollution Research*, vol. 29, no. 28, pp. 42539–42559, 2022. https://doi.org/10.1007/s11356-022-19718-6

[5] R. Levy, T. Naish, D. Lowry *et al.*, "Melting ice and rising seas—Connecting projected change in Antarctica's ice sheets to communities in Aotearoa New Zealand," *Journal of the Royal Society of New Zealand*, vol. 54, no. 4, pp. 449–472, 2024. https://doi.org/10.1080/03036758.2023.2232743

[6] C. A. Deutsch, J. J. Tewksbury, M. Tigchelaar *et al.*, "Increase in crop losses to insect pests in a warming climate," *Science*, vol. 361, no. 6405, pp. 916–919, 2018. https://doi.org/10.1126/science.aat3466

[7] G. S. Malhi, M. Kaur, and P. Kaushik, "Impact of climate change on agriculture and its mitigation strategies: A review," *Sustainability*, vol. 13, no. 3, 1318, 2021. https://doi.org/10.3390/su13031318

[8] R. Wall and L. S. Ellse, "Climate change and livestock parasites: Integrated management of sheep blowfly strike in a warmer environment," *Global Change Biology*, vol. 17, no. 5, pp. 1770–1777, 2011. https://doi.org/10.1111/j.1365-2486.2010.02361.x

[9] H. M. Moda, W. L. Filho, and A. Minhas, "Impacts of climate change on outdoor workers and their safety: Some research priorities," *International Journal of Environmental Research and Public Health*, vol. 16, no. 18, 3458, 2019. https://doi.org/10.3390/ijerph16183458

[10] C. Caminade, K. M. McIntyre, and A. E. Jones, "Impact of recent and future climate change on vector-borne diseases," *Annals of the New York Academy of Sciences*, vol. 1436, no. 1, pp. 157–173, 2019. https://doi.org/10.1111/nyas.13950

[11] P. A. Owusu and S. Asumadu-Sarkodie, "A review of renewable energy sources, sustainability issues and climate change mitigation," *Cogent Engineering*, vol. 3, no. 1, 1167990, 2016. https://doi.org/10.1080/23311916.2016.1167990

[12] A. Jordan, R. K. W. Wurzel, and A. Zito, "The rise of 'new' policy instruments in comparative perspective: Has governance eclipsed government?" *Political Studies*, vol. 53, no. 3, pp. 477–496, 2005. https://doi.org/10.1111/j.1467-9248.2005.00540.x

[13] Intergovernmental Panel on Climate Change (IPCC), *Climate Change 2021—The Physical Science Basis: Working Group I Contribution to the Sixth Assessment Report of the Intergovernmental Panel on Climate Change*, Cambridge, UK: Cambridge University Press, 2023. https://doi.org/10.1017/9781009157896

[14] M. Kabir, U. Habiba, M. Z. Iqbal *et al.*, "Impacts of anthropogenic activities & climate change resulting from increasing concentration of carbon dioxide on environment in 21st century; A critical review," in *Proc. IOP Conference Series: Earth and Environmental Science*, 2023, vol. 1194, no. 1, 012010. https://doi.org/10.1088/1755-1315/1194/1/012010

[15] F. W. Taylor, "The greenhouse effect and climate change," *Reports on Progress in Physics*, vol. 54, no. 6, pp. 881–918, 1991. https://doi.org/10.1088/0034-4885/54/6/002

[16] I. Mehmood, A. Bari, S. Irshad *et al.*, "Carbon cycle in response to global warming," in *Environment, Climate, Plant and Vegetation Growth*, Cham, Switzerland: Springer International Publishing, 2020, pp. 1–15. https://doi.org/10.1007/978-3-030-49732-3_1

[17] W. F. Lamb, T. Wiedmann, J. Pongratz *et al.*, "A review of trends and drivers of greenhouse gas emissions by sector from 1990 to 2018," *Environmental Research Letters*, vol. 16, no. 7, 073005, 2021. https://doi.org/10.1088/1748-9326/abee4e

[18] L. J. R. Nunes, "The rising threat of atmospheric CO_2: A Review on the causes, impacts, and mitigation strategies," *Environments*, vol. 10, no. 4, p. 66, 2023. https://doi.org/10.3390/environments10040066

[19] A. V. Strizhenok, M. V. Bykova, and A. E. Korotaeva, "Extractive industries as a source of greenhouse gas emissions and the possibility of its natural sequestration under the climatic conditions of Central and Northern Eurasia," *Journal of Ecological Engineering*, vol. 25, no. 5, 2024. https://doi.org/10.12911/22998993/185585

[20] N. Jones, "Troubling milestone for CO_2," *Nature Geoscience*, vol. 6, no. 8, pp. 589–589, 2013. https://doi.org/10.1038/ngeo1900

[21] I. Hussain, H. Alasiri, W. U. Khan *et al.*, "Advanced electrocatalytic technologies for conversion of carbon dioxide into methanol by electrochemical reduction: Recent progress and future perspectives," *Coordination Chemistry Reviews*, vol. 482, 215081, 2023. https://doi.org/10.1016/j.ccr.2023.215081

[22] Z. Turakulov, A. Kamolov, A. Norkobilov *et al.*, "Assessing various CO_2 utilization technologies: A brief comparative review," *Journal of Chemical Technology & Biotechnology*, vol. 99, no. 6, pp. 1291–1307, 2024. https://doi.org/10.1002/jctb.7606

[23] Z. Amiri, A. Heidari and N. J. Navimipour, "Comprehensive survey of artificial intelligence techniques and strategies for climate change mitigation," *Energy*, vol. 308, 132827, 2024. https://doi.org/10.1016/j.energy.2024.132827

[24] S. Materia, L. P. García, C. van Straaten *et al.*, "Artificial intelligence for climate prediction of extremes: State of the art, challenges, and future perspectives," *WIREs Climate Change*, vol. 15, no. 6, 2024. https://doi.org/10.1002/wcc.914

[25] M. I. Jordan and T. M. Mitchell, "Machine learning: Trends, perspectives, and prospects," *Science*, vol. 349, no. 6245, pp. 255–260, 2015. https://doi.org/10.1126/science.aaa8415

[26] S. Dargan, M. Kumar, M. R. Ayyagari, and G. Kumar, "A survey of deep learning and its applications: A new paradigm to machine learning," *Archives of Computational Methods in Engineering*, vol. 27, no. 4, pp. 1071–1092, 2020. https://doi.org/10.1007/s11831-019-09344-w

[27] I. H. Sarker, "Machine learning: Algorithms, real-world applications and research directions," *SN Computer Science*, vol. 2, no. 3, pp. 1–21, 2021. https://doi.org/10.1007/s42979-021-00592-x

[28] R. K. Inapakurthi, S. S. Miriyala, and K. Mitra, "Deep learning based dynamic behavior modelling and prediction of particulate matter in air," *Chemical Engineering Journal*, vol. 426, 131221, 2021. https://doi.org/10.1016/j.cej.2021.131221

[29] S. W. Fleming and A. G. Goodbody, "A machine learning metasystem for robust probabilistic nonlinear regression-based forecasting of seasonal water availability in the US west," *IEEE Access*, vol. 7, pp. 119943–119964, 2019. doi: 10.1109/ACCESS.2019.2936989

[30] M. S. Zaghloul and G. Achari, "Application of machine learning techniques to model a full-scale wastewater treatment plant with biological nutrient removal," *Journal of Environmental Chemical Engineering*, vol. 10, no. 3, 107430, 2022. https://doi.org/10.1016/j.jece.2022.107430

[31] M. Chierici, M. Giulini, N. Bussola *et al.*, "Machine learning models for predicting endocrine disruption potential of environmental chemicals," *Journal of Environmental Science and Health, Part C*, vol. 36, no. 4, pp. 237–251, 2018. https://doi.org/10.1080/10590501.2018.1537155

[32] L. Chen, Z. Chen, Y. Zhang *et al*., "Artificial intelligence-based solutions for climate change: A review," *Environmental Chemistry Letters*, vol. 21, no. 5, pp. 2525–2557, 2023. https://doi.org/10.1007/s10311-023-01617-y

[33] S. Krishnamurthy, O. B. Adewuyi, and S. A. Salimon, "Recent advances in artificial intelligence-based optimization for power system applications: A review of techniques, challenges, and future directions" *Renewable and Sustainable Energy Reviews*, vol. 226, 116340, 2026. https://doi.org/10.1016/j.rser.2025.116340

[34] D. Fister, J. Pérez-Aracil, C. Peláez-Rodríguez *et al.*, "Accurate long-term air temperature prediction with machine learning models and data reduction techniques," *Applied Soft Computing*, vol. 136, 110118, 2023. https://doi.org/10.1016/j.asoc.2023.110118

[35] M. K. Nematchoua, J. A. Orosa, and M. Afaifia, "Prediction of daily global solar radiation and air temperature using six machine learning algorithms; A case of 27 European countries," *Ecological Informatics*, vol. 69, 101643, 2022. https://doi.org/10.1016/j.ecoinf.2022.101643

[36] X. Ding, Y. Zhao, Y. Fan *et al.*, "Machine learning-assisted mapping of city-scale air temperature: Using sparse meteorological data for urban climate modeling and adaptation," *Building and Environment*, vol. 234, 110211, 2023. doi: 10.1016/j.buildenv.2023.110211

[37] H. Wang, J. Yang, G. Chen *et al.*, "Machine learning applications on air temperature prediction in the urban canopy layer: A critical review of 2011–2022," *Urban Climate*, vol. 49, 101499, 2023. https://doi.org/10.1016/j.uclim.2023.101499

[38] J. J. Aguilera, R. K. Andersen, and J. Toftum, "Prediction of indoor air temperature using weather data and simple building descriptors," *International Journal of Environmental Research and Public Health*, vol. 16, no. 22, 4349, 2019. https://doi.org/10.3390/ijerph16224349

[39] J. Soyemi and A. Adesola, "A web-based decision support system with SMS-based technology for agricultural information and weather forecasting," *International Journal of Computer Applications*, vol. 180, no. 16, pp. 1–6, 2018. https://doi.org/10.5120/ijca2018916338

[40] S. Suryono, R. Saputra, B. Sularso *et al.*, "Web-based fuzzy time series for environmental temperature and relative humidity prediction," in *Proc. 2017 IEEE International Conference on Communication, Networks and Satellite (Comnetsat)*, 2017, pp. 36–41. https://doi.org/10.1109/comnetsat.2017.8263570

[41] A. Perera and U. Rathnayake, "Rainfall and atmospheric temperature against the other climatic factors: A case study from Colombo, Sri Lanka," *Mathematical Problems in Engineering*, vol. 2019, no. 1, 2019. https://doi.org/10.1155/2019/5692753

[42] Y. Wang, Y. Bai, L. Yang, and H. Li, "Short time air temperature prediction using pattern approximate matching," *Energy and Buildings*, vol. 244, 111036, 2021. doi: 10.1016/j.enbuild.2021.111036

[43] S. Liu, J. McGree, Z. Ge, and Y. Xie, "Classification methods," in *Computational and Statistical Methods for Analysing Big Data with Applications*, Academic Press, 2016, pp. 7–28. https://doi.org/10.1016/B978-0-12-803732-4.00002-7

[44] J. R. Quinlan, "Induction of decision trees," *Machine Learning*, vol. 1, no. 1, pp. 81–106, 1986. https://doi.org/10.1007/BF00116251

[45] D. P. P. Meddage, I. U. Ekanayake, A. U. Weerasuriya *et al.*, "Explainable Machine Learning (XML) to predict external wind pressure of a low-rise building in urban-like settings," *Journal of Wind Engineering and Industrial Aerodynamics*, vol. 226, 105027, 2022. https://doi.org/10.1016/j.jweia.2022.105027

[46] L. Breiman, "Random forests," *Machine Learning*, vol. 45, pp. 5–32, 2001. https://doi.org/10.1023/A:1010933404324

[47] L. Breiman, "Bagging predictors," *Machine Learning*, vol. 24, no. 2, pp. 123–140, 1996. https://doi.org/10.1007/BF00058655

[48] R. Genuer, J. M. Poggi, and C. Tuleau-Malot, "Variable selection using random forests," *Pattern Recognition Letters*, vol. 31, no. 14, pp. 2225–2236, 2010. https://doi.org/10.1016/j.patrec.2010.03.014

[49] A. Afradi, A. Ebrahimabadi, and T. Hallajian, "Prediction of the penetration rate and number of consumed disc cutters of Tunnel Boring Machines (TBMs) using Artificial Neural Network (ANN) and Support Vector Machine (SVM)—Case study: Beheshtabad water conveyance tunnel in Iran," *Asian Journal of Water, Environment and Pollution*, vol. 16, no. 1, pp. 49–57, 2019. https://doi.org/10.3233/AJW190006

[50] H. Moosaei, F. Bazikar, and M. Hladík, "Universum parametric v-support vector regression for binary classification problems with its applications," *Annals of Operations Research*, pp. 1–45, 2023. https://doi.org/10.1007/s10479-023-05369-4

[51] M. Awad and R. Khanna, "Support vector regression," in *Efficient Learning Machines: Theories, Concepts, and Applications for Engineers and System Designers*, Berkeley, CA: Apress, 2015, pp. 67–80. https://doi.org/10.1007/978-1-4302-5990-9_4

[52] F. Kazemi, N. Asgarkhani, and R. Jankowski, "Machine learning-based seismic fragility and seismic vulnerability assessment of reinforced concrete structures," *Soil Dynamics and Earthquake Engineering*, vol. 166, 107761, 2023. https://doi.org/10.1016/j.soildyn.2023.107761

[53] S. Sun, M. Guillen, A. M. Pérez-Marín, and L. Ni, "Determining driving risk factors from near-miss events in telematics data using histogram-based gradient boosting regressors," *Journal of Theoretical and Applied Electronic Commerce Research*, vol. 19, no. 4, pp. 3477–3497, 2024. https://doi.org/10.3390/jtaer19040169

[54] A. Božič, "Relationship between indoor and outdoor temperature and humidity in a residential building in Central Europe," *Discover Environment*, vol. 2, no. 1, 63, 2024. https://doi.org/10.1007/s44274-024-00104-7

[55] M. A. Ali, A. Elsayed, I. Elkabani *et al.*, "Modeling global solar radiation using ambient temperature," *Cleaner Energy Systems*, vol. 7, 100101, 2024. https://doi.org/10.1016/j.cles.2023.100101

[56] J. A. Acero, P. Kestel, H. T. Dang *et al*., "Impact of rainfall on air temperature, humidity and thermal comfort in tropical urban parks," *Urban Climate*, vol. 56, 102051, 2024. https://doi.org/10.1016/j.uclim.2024.102051

[57] D. A. Sachindra and M. Nowosad, "Characteristics of wind speeds and outdoor thermal sensation considering the effect of wind speeds: An analysis based on hourly data from 1995 to 2021 in Poland," *International Journal of Climatology*, vol. 42, no. 16, pp. 10021–10047, 2022. https://doi.org/10.1002/joc.7880

[58] M. Kabir, U. E. Habiba, W. Khan *et al*., "Climate change due to increasing concentration of carbon dioxide and its impacts on environment in 21st century; a mini review," *Journal of King Saud University-Science*, vol. 35, no. 5, 102693, 2023. https://doi.org/10.1016/j.jksus.2023.102693

[59] S. Al-jaf and O. T. Al-Taai, "Impact of nitrous oxide (N2O) concentrations on atmospheric air temperature changes over Iraq and some neighboring regions," *Journal of Garmian University*, vol. 6, no. 3, pp. 338–348, 2019. https://doi.org/10.24271/garmian.196360

[60] N. Rößger, T. Sachs, C. Wille *et al.*, "Seasonal increase of methane emissions linked to warming in Siberian tundra," *Nature Climate Change*, vol. 12, no. 11, pp. 1031–1036, 2022. https://doi.org/10.1038/s41558-022-01512-4

[61] Y. Gu, K. Li, J. Xu *et al.*, "Observed dependence of surface ozone on increasing temperature in Shanghai, China," *Atmospheric Environment*, vol. 221, 117108, 2020. https://doi.org/10.1016/j.atmosenv.2019.117108

[62] Z. Liu, H. Meng, X. Wang *et al*., "Interaction between ambient CO and temperature or relative humidity on the risk of stroke hospitalization," *Scientific Reports*, vol. 14, no. 1, 16740, 2024. https://doi.org/10.1038/s41598-024-67568-8

[63] M. L. P. Leão, L. Zhang, and F. M. R. da Silva Júnior, "Effect of particulate matter (PM2.5 and PM10) on health indicators: Climate change scenarios in a Brazilian metropolis," *Environmental Geochemistry and Health*, vol. 45, no. 5, pp. 2229–2240, 2023. https://doi.org/10.1007/s10653-022-01331-8

[64] M. Li, H. Sun, Y. Huang *et al*., "Shapley value: From cooperative game to explainable artificial intelligence," *Autonomous Intelligent Systems*, vol. 4, no. 1, 2024. https://doi.org/10.1007/s43684-023-00060-8

[65] H. Sahlaoui, A. Nayyar, S. Agoujil *et al.*, "Predicting and interpreting student performance using ensemble models and shapley additive

explanations," *IEEE Access*, vol. 9, 152688–152703, 2021. https://doi.org/10.1109/ACCESS.2021.3124270

[66] D. Kerrigan, B. Barr, and E. Bertini, "PDPilot: Exploring partial dependence plots through ranking, filtering, and clustering," *IEEE Transactions on Visualization and Computer Graphics*, vol. 31, no. 10, pp. 7377–7390, 2025. https://doi.org/10.1109/TVCG.2025.3545025

[67] Y. Peng and C. Unluer, "Interpretable machine learning-based analysis of hydration and carbonation of carbonated reactive magnesia cement mixes," *Journal of Cleaner Production*, vol. 434, 140054, 2024. https://doi.org/10.1016/j.jclepro.2023.140054

[68] M. Á. Fernández-Centeno, P. Alocén, and M. Á. Toledo, "Identification of trends in dam monitoring data series based on machine learning and individual conditional expectation curves," *Water*, vol. 16, no. 9, 1239, 2024. https://doi.org/10.3390/w16091239

[69] U. Orji and E. Ukwandu, "Machine learning for an explainable cost prediction of medical insurance," *Machine Learning with Applications*, vol. 15, 100516, 2024. https://doi.org/10.1016/j.mlwa.2023.100516

[70] K. Shabbir, M. Noureldin, and S. Sim, "Data-driven model for seismic assessment, design, and retrofit of structures using explainable artificial intelligence," *Computer-Aided Civil and Infrastructure Engineering*, vol. 40, no. 3, pp. 281–300, 2025. https://doi.org/10.1111/mice.13338

[71] D. W. Apley and J. Zhu, "Visualizing the effects of predictor variables in black box supervised learning models," *Journal of the Royal Statistical Society Series B: Statistical Methodology*, vol. 82, no. 4, pp. 1059–1086, 2020. https://doi.org/10.1111/rssb.12377

[72] C. Molnar, G. Casalicchio, and B. Bischl, "Quantifying model complexity via functional decomposition for better post-hoc interpretability," in *Proc. Joint European Conference on Machine Learning and Knowledge Discovery in Database*, 2019, pp. 193–204. https://doi.org/10.1007/978-3-030-43823-4_17

[73] C. Okoli. 2023. ale: Interpretable machine learning and statistical inference with Accumulated Local Effects (ALE). [Online]. Available: https://doi.org/10.32614/cran.package.ale

[74] Z. Wang and A. C. Bovik, "Mean squared error: Love it or leave it? A new look at signal fidelity measures," *IEEE Signal Processing Magazine*, vol. 26, no. 1, pp. 98–117, 2009. https://doi.org/10.1109/msp.2008.930649

[75] D. Chicco, M. J. Warrens, and G. Jurman, "The coefficient of determination R-squared is more informative than SMAPE, MAE, MAPE, MSE and RMSE in regression analysis evaluation," *PeerJ Computer Science*, vol. 7, e623, 2021. https://doi.org/10.7717/peerj-cs.623

[76] H. Sajindra, S. Dharmawansha, H. Wijesundara *et al.*, "Hybrid neural network methods to model the external wind pressure on a low-rise flat-roofed building in an irregularly shaped urban environment," *Structures*, vol. 79, 109529, 2025. https://doi.org/10.1016/j.istruc.2025.109529

[77] T. Abekoon, H. Sajindra, N. Rathnayake *et al.*, "A novel application with explainable machine learning (shap and lime) to predict soil N, P, and K nutrient content in cabbage cultivation," *Smart Agricultural Technology*, vol. 11, 100879, 2025. https://doi.org/10.1016/j.atech.2025.100879